JOURNAL OF THERMOPHYSICS AND HEAT TRANSFER
Vol. 8, No. 1, Jan.–March 1994

# Modeling a Horizontal Heat-Flux Cylinder as a Line Source

Valérie Deschamps*
*Conservatoire National des Arts et Métius, Paris 75141, France*
and
Gilles Desrayaud†
*IBM, Montpellier 34820, France*

**A numerical investigation of convective plumes above horizontal heat-flux cylinders immersed in the vertical centerplane of rectangular air-filled vessels has been carried out. In this article, the heated wire was modeled using two approaches: 1) as a heat source term in the energy equation and 2) as a cylinder of finite-diameter. Comparisons between the two strategies are done for local values of flow variables and integrated ones for steady-state motions. Good agreements were obtained in the boundary-layer regime while great discrepancies appeared in the conduction and transition regime for which heat is mainly transferred by conduction. Periodic motions have also been investigated and very good agreements were found in general trends of unsteady flows whatever the Rayleigh number. It is concluded that for dimensions of the enclosures, which largely compared with the cylinder radius, the heat source term model is a promising way to study the behavior of unsteady plume flows owing to its simplicity, flexibility, and low computational costs.**

## Nomenclature

$A$ = vertical aspect ratio, $H/D$
$a$ = thermal diffusivity
$D$ = width of the vessel
$d$ = dimensionless cylinder diameter
$f$ = frequency of time-dependent motion
$g$ = gravitational acceleration
$H$ = height of the vessel
$H_s$ = depth of immersion, $A - y_s$
$Pr$ = Prandtl number, $\nu_0/a_0$
$p$ = pressure
$Q$ = heat generated per unit length of line source
$Ra$ = Rayleigh number, $g\beta QD^3/\lambda_0 a_0 \nu_0$
$T$ = temperature
$T_a$ = ambient temperature
$t$ = time
$V$ = velocity vector of components $(U, V)$
$x, y$ = coordinates
$\beta$ = volumetric thermal expansion coefficient
$\Delta t$ = dimensionless time step
$\theta$ = dimensionless temperature, $\lambda_0(T - T_a)/Q$
$\lambda$ = thermal conductivity
$\mu$ = fluid viscosity
$\nu$ = kinematic fluid viscosity
$\rho$ = fluid density
$\phi$ = dimensionless heat flux through a horizontal plane $y$
$\psi$ = stream function
$\omega$ = heat generation rate per unit volume

*Subscripts*
$s$ = refers to line source
0 = for reference temperature

*Superscript*
$'$ = dimensional quantity

Received July 23, 1992; revision received March 16, 1993; accepted for publication March 23, 1993. 

*Graduate Student, Laboratoire de Thermique, 292 rue Saint-Martin.

†Research Scientist; currently at Centre National Universitaire Sud de Calal, 950 route de Saint Priest, 34184 Montpellier Cedex 4, C3NI.

## Introduction

FREELY-RISING plume from horizontal line heat source in fluids has been studied extensively since the early similarity analysis of Fujii.[1] Several studies have focused on the dynamical behavior of such a system. These have been carried out both experimentally and theoretically on the basis of linear stability analysis. Extensive reviews of these studies have been presented by Gebhart et al.[2] Only few recent experimental works have been devoted to buoyancy induced flow inside fluid-filled vessels: some considered the case of a line source,[3–5] whereas others investigated the case of immersed isothermal cylinder.[6–8] The pronounced dynamical feature of a freely rising plume is a regular naturally swaying motion of the entire plume in a plane perpendicular to the axis of the line source. It has been observed experimentally in liquids (water and spindle oil) and in air[9,10] for heating rate exceeding a threshold value that depends strongly on the thermophysical properties of the fluid and environmental conditions, such as the isolation of the test vessels and the depth of immersion. The dynamical boundary conditions applied at the upper surface (free surface or rigid surface) do not appear to play a significant role.[8]

Another mode of instability, a meandering motion along the heater direction (across the span of the plane plume) has also been observed. These two motions, swaying and meandering, are not independent of each other.[4,8] The physical mechanisms leading the plume to meander are yet unclarified and in many experiments this motion did not appear.[3,5,11,12] The existence of this meandering motion is claimed by Noto[5] to be related to the width of the vessel, but he seems not to offer any experimental proof.

To the authors' knowledge, numerical studies of confined plumes are sparse. Recently, G. Desrayaud and G. Lauriat have investigated the route to chaos of thermal plumes in rectangular vessels.[13,14] It has been shown that the thermal boundary conditions play only a minor role on the steady-state flows structure[13] and on oscillatory behavior of periodic motions.[14]

Although most plumes occurring in the environment are turbulent, it is felt that further study of the behavior of laminar plumes is justified. Indeed, since many numerical codes developed to study laminar flows are now used for direct simulations of chaotic or weakly turbulent flows, it is important to ascertain how these laminar models behave. Of course, direct simulations are very time-consuming, even running on powerful vector computers. Therefore, simplifications of the

complexity in the governing equations, or in the formulations, are not only helpful, but required. Our ultimate purpose is to develop a reliable numerical scheme which would be fast enough to investigate laminar-turbulent transition plume flows and three-dimensional parametric study.

To achieve this goal, the wire is modeled as a local source term in the energy equation. Other strategies have been employed, such as boundary-fitted coordinates[15] or finite elements method, to model a cylinder, but at the expense of additional complexity in the governing equations and formulations, respectively. A polar grid has also been used in the vicinity of the cylinder.[16] It gives better control of grid locations, but has the disadvantage of the presence of an overlapping zone between the polar and Cartesian grids, and of somewhat arbitrary conditions where they meet. Another advantage of the local heat source term strategy is its inherent flexibility, for it allows the heat source to be readily moved and, e.g., thermal interactions between two or more line sources inside vessels to be easily studied.

In this article, a wire inside rectangular vessels is modeled as a source term in the energy equation and comparisons with a wire modeled as a finite-diameter cylinder of constant heat flux are dealt with. Buoyant plumes induced by a wire inside a square vessel are considered first for steady and periodic flows. A complete discussion of the bifurcations which occur in rectangular vessels owing to the aspect ratio and the depth of immersion can be found in the paper by Desrayaud and Lauriat.[14] Some comparisons in rectangular vessels of aspect ratio 2 for which different kinds of bifurcation occur at low Rayleigh numbers are also presented.

## Mathematical Formulation

Consider a two-dimensional fluid-filled vessel of $D$ and $H$, enclosed by adiabatic vertical walls and isothermally cooled horizontal surfaces at $T_a$, as shown in Fig. 1. A wire which generates a heat flux $Q$ per unit length is immersed at the central vertical plane $(x_s', y_s')$ of the vessel.

For a Boussinesq fluid, the conservation equations for mass, momentum, and energy are reduced in the dimensionless form to[13]

$$\nabla \cdot \boldsymbol{V} = 0 \tag{1}$$

$$\frac{1}{Pr}\left[\frac{\partial \boldsymbol{V}}{\partial t} + (\boldsymbol{V}\cdot\nabla)\boldsymbol{V}\right] = -\nabla p + \nabla^2 \boldsymbol{V} + Ra\theta \boldsymbol{k} \tag{2}$$

$$\frac{\partial \theta}{\partial t} + (\boldsymbol{V}\cdot\nabla)\theta = \nabla^2\theta + \omega \tag{3}$$

The Prandtl number and the Rayleigh number are $Pr = \nu_0/a_0$ and $Ra = g\beta QD^3/\lambda_0\nu_0 a_0$.

The dimensionless form of Eqs. (1–3) has been obtained by scaling lengths, time, and temperature difference $(T - T_a)$ by $D$, $D^2/a_0$, and $Q/\lambda_0$, respectively. As a result, the relevant hydrodynamic and thermal boundary conditions can be written in the following dimensionless form:

$$\boldsymbol{V} = 0 \quad \text{on all boundary} \tag{4a}$$

$$\frac{\partial \theta}{\partial x} = 0 \quad \text{at} \quad x = 0, 1 \tag{4b}$$

$$\theta = 0 \quad \text{at} \quad y = 0, A \tag{4c}$$

where $A = H/D$ is the aspect ratio of the cross section of the vessel.

To model a pipe as a line source, Beck et al.[17] used Green's functions and developed a transient solution to describe heat conduction transfer around a single buried steam pipe inside a semi-infinite medium. Then, the basic idea of modeling the wire as a source term in the energy equation is to cast $\omega$ as follows:

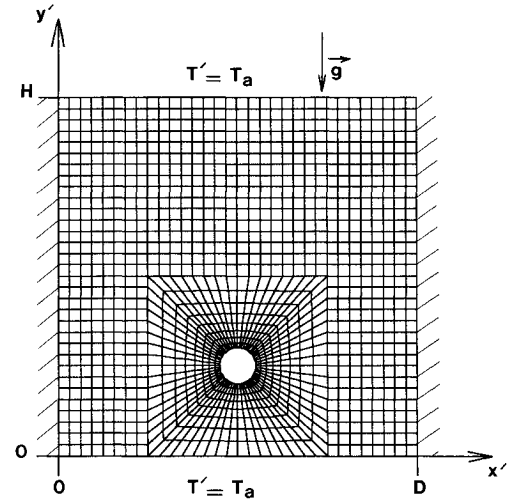


**Fig. 1 Coordinate system and finite element grid, $A = 1$, $H_s = 0.75$.**

$$\omega = \delta(x_s - x)\delta(y_s - y) \tag{5}$$

where $\delta(z)$ is the Dirac delta function. The integral of $\delta(x_s - x)\delta(y_s - y)$ over $x$ and $y$ equal unity, if it includes $(x_s, y_s)$; otherwise it is zero.

At steady state, the energy dissipated by the line heat source is lost at the boundaries. This requirement of equality leads to the nondimensional steady-state condition

$$\int_{\mathbb{D}} \delta(x_s - x)\delta(y_s - y)\, dS = 1 = -\int_{\Gamma} \frac{\partial \theta}{\partial n}\, d\Gamma \tag{6}$$

where $\mathbb{D}$ is the problem domain and $\Gamma$ the boundary.

In addition, the heat flux through any horizontal plane $y$, defined as

$$\phi(y) = \int_0^1 \left(-\frac{\partial \theta}{\partial y} + V\theta\right) dx \tag{7}$$

must satisfy the following conditions:

$$\phi(y^-) + \phi(y^+) = 1 \qquad \forall y^- < y_s \quad \text{and} \quad \forall y^+ > y_s \tag{8}$$

On the other hand, if the wire is considered as a cylinder of dimensionless finite diameter $d$ centered on $(x_s, y_s)$, the following thermal boundary condition must be added:

$$\frac{\partial \theta}{\partial n} = 1 \qquad \text{on the cylinder boundary} \tag{9}$$

with no-slip boundary conditions and obviously $\omega = 0$ in the energy equation.

## Numerical Method

In the case of a local source term, the solution technique has been described in a previous paper[13] and is briefly mentioned here. The governing equations were written in the stream function vorticity formulation and discretized by a finite difference method of second-order accuracy. Convective terms are discretized by employing central differences. The vorticity and energy equation were solved in transient form and the time integration was performed using an alternating direction implicit (ADI) splitting scheme. The nodal points of the vorticity and stream function were located on a standard mesh. For the energy equation, a control-volume formulation with staggered grids and central differencing was

retained. The discretized equations for the stream function equation were solved by a block-cyclic reduction process.[18] From the solution of the stream function equation, the wall vorticity was updated using second-order accurate formulation.

The computer code has been successfully employed by G. Desrayaud to study unsteady free convection heat transfer in a shallow cavity.[19] The applicability of the method and its accuracy for this type of problem has been found to be very satisfactory when compared to finite volume, finite element, and spectral methods.[20] Furthermore, an experimental correlation, $f \propto Ra^{0.4}$, has been given by Noto[5] for confined laminar plumes in rectangular vessel of aspect ratio $A = 1.25$ and depth of immersion $H_s = 0.75$. Using the same finite difference computational code as the one used here, Desrayaud and Lauriat[14] numerically found a 0.405 power. This gives us confidence in the reliability of the numerical code.

Most of the computations reported here have been performed on an IBM 3090 600/VF vector computer. For typical cases, the vectorized performance (ratio of scalar to vectorial CPU time) was only slightly greater than 2. The reason for this is mainly due to the difficulties in vectorizing the bloccyclic reduction solver. When using an ADI scheme to solve the Poisson equation of the stream function, the vectorized performance was over 3. However, it is preferable not to introduce an internal iterative procedure when accurate transient motions are followed.

A commercial fluid dynamics analysis package, FIDAP,[21] was also used for solving the governing PDEs in the primitive variable formulation, Eqs. (1–3), with the boundary conditions given by Eqs. (4) and (9). While finite elements are CPU time consuming, the modeling of a cylinder inside a rectangular vessel is straightforward. This is why a finite element software package was chosen. In the present study, the four-node quadrilateral finite element is used for velocity and temperature variables with piecewise constant pressure. A penalty function approximation has been chosen for the computation of the pressure. Integrals are evaluated exactly using one point Gaussian quadrature. At every selected Rayleigh number, the successive substitution method is used for the first three iterations for solving the system of nonlinear equations, and the Newton-Raphson method is chosen after the third iteration. With these combinations, solutions converge smoothly to a 0.1% convergence criterion of the relative velocity and residuals within six to seven iterations for all steps. The selected penalty constant is $10^{-8}$ for all cases and Rayleigh numbers.

Finite element meshes are built over a Cartesian 33 × 33 grid and cylindrical mesh refinement is only used near the cylinder (Fig. 1). Indeed, mesh refinement is needed in the vicinity of the cylinder when decreasing its size in order to maintain the accuracy of the results, the four-node quadrilateral elements being straight-sided. Thus, 1152 elements are used for the 1/10 diameter while there are 1664 elements for $d = 1/100$. A consequence of mesh refinement is that, after the three successive substitution iterations, four Newton-Raphson iterations are needed to reach convergence criterion for $d = 1/100$ instead of three for greater diameters. Thus, the elapsed CPU time greatly increased for very small diameters.

For transient problems, the time integration was performed by the combination of two second-order accurate techniques: 1) the implicit trapezoid rule for the velocity and 2) an explicit Adams-Bashforth formula for the pressure. If the solution at each time step is reasonably close to the solution at the previous time step, a one-step Newton-Raphson method can be used to solve the nonlinear system of algebraic equations. Typically, a value of $\Delta t = 0.003$ was used at $Ra = 3 \times 10^7$ in a square vessel for a cylinder having a diameter of 1/70. All the finite elements computations were performed on a entry level superscalar workstation.

## Results and Discussion

### Square Vessels

Temperature and velocity fields of steady convection around a heated wire immersed at $H_s = A - y_s = 0.75$ in square vessels are presented in Fig. 2 for two different Rayleigh numbers. Isotherms are shown on the right side and streamlines on the left side of the figure. The motion is characterized by two counter-rotating cells induced by recirculations in which warm fluid rises with the plume above the line-source, is cooled downstream and descends along the adiabatic sides. The highest velocity and temperature gradients are located around the wire and in the plume itself. In square vessels and for a line heat source immersed in the central vertical plane at a depth of immersion $H_s = 0.75$, it has been shown[13] that steady flows exist up to $Ra \cong 3 \times 10^7$.

Superpositions of temperature and stream function fields are also presented in Fig. 2 for $Ra = 10^5$ and $Ra = 10^7$ for the case of a source term of 1/32 × 1/32 square surface and a cylinder of 1/70 diameter. As can be seen, the temperature fields near the top surface are in good agreement, whereas some discrepancies appear in the vicinity of the heat source, where the temperature gradient is the highest. Also, on the stream function fields the centers of the rolls move upward when increasing the Rayleigh number, and the layer below the source is increasingly more stagnant. The twisting of the streamlines is smooth near the cylinder. Thus, flowfields compare well, the comparison being slightly better for $Ra = 10^7$ (Fig. 2b) than for $Ra = 10^5$ (Fig. 2a), especially in the vicinity of the cylinder.

#### *Steady Flows*

This section addresses the minimum number of grid points required to obtain solutions that are reasonably grid-independent for the case of a line heat source. To this end, the effect of the mesh size on the solutions is documented in Table 1 for $Ra = 10^5$, $10^6$, and $10^7$. The computations were carried out on 33 × 33, 65 × 65, and 129 × 129 regular meshes. For Rayleigh numbers below the critical value ($Ra \cong 3 \times 10^7$), the solutions (except for the source temperature, $\theta_s$) for the two finest meshes are within 1% for local and integrated values. Indeed, since the heat is introduced in one control

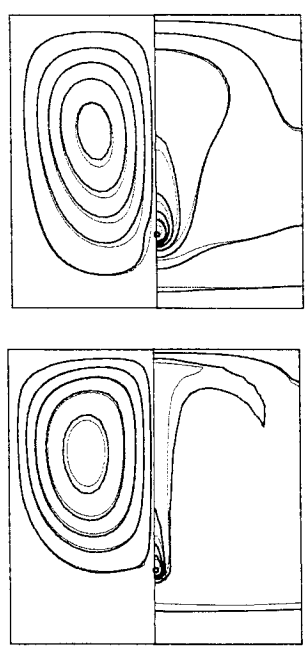


**Fig. 2 Streamlines and isotherms in a square vessel, $H_s = 0.75$ (thin lines are for local heat source while thick lines are for 1/70 cylinder): a) $Ra = 10^5$ and b) $Ra = 10^7$.**

**Table 1 Comparison of some characteristic values for different Rayleigh numbers in a square vessel and for a depth of immersion $H_s = 0.75$ in the case of a line heat source**

| $Ra$ | Grid | $\psi_{max}$ | $\bar{\phi}$ | $\theta_s$ | $U_1$ | $V_1$ | $V_2$ | $T_2$ |
|---|---|---|---|---|---|---|---|---|
| | 33 × 33 | 6.13 | 0.6878 | 0.281 | 9.88 | −12.46 | 36.54 | 0.140 |
| $10^5$ | 65 × 65 | 6.14 | 0.6872 | 0.376 | 10.13 | −12.75 | 36.58 | 0.141 |
| | 129 × 129 | 6.14 | 0.6870 | 0.480 | 10.19 | −12.83 | 36.59 | 0.141 |
| | 33 × 33 | 18.52 | 0.8134 | 0.125 | 43.55 | −21.93 | 145.1 | 0.085 |
| $10^6$ | 65 × 65 | 18.53 | 0.8116 | 0.250 | 44.59 | −22.33 | 147.0 | 0.086 |
| | 129 × 129 | 18.56 | 0.8112 | 0.343 | 44.87 | −22.43 | 147.4 | 0.086 |
| | 33 × 33 | 46.05 | 0.8858 | 0.102 | 81.11 | −32.91 | 409.8 | 0.052 |
| $10^7$ | 65 × 65 | 46.45 | 0.8806 | 0.157 | 78.91 | −32.52 | 425.3 | 0.055 |
| | 129 × 129 | 46.60 | 0.8794 | 0.231 | 78.96 | −32.43 | 429.3 | 0.055 |

Subscripts 1 and 2 are for the points $M_1(0.25, A/2)$ and $M_2(0.5, 3A/4)$, respectively.

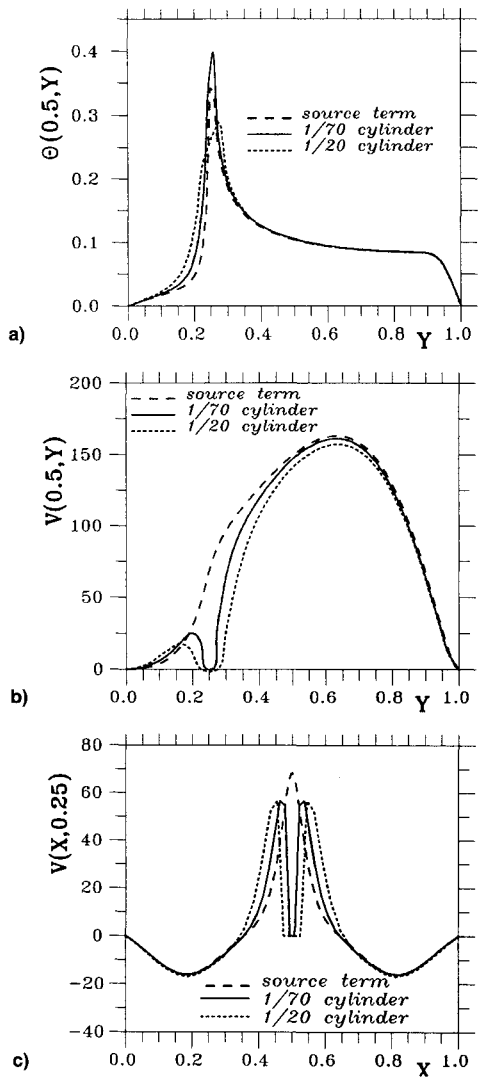


**Fig. 3 Profile of some variables at $Ra = 10^6$ for two different cylinder diameters and a line heat source of 1/64 × 1/64 surface: a) temperature profile on the vertical centerplane, b) vertical component of the velocity on the vertical centerplane, and c) vertical component of the velocity on the horizontal plane of the wire.**

volume only, the temperature and flowfield in the immediate vicinity of the heat source cannot be grid independent. The source temperature must tend to infinity as the area of the control volume tends to zero. The decrease in the source temperature when the Rayleigh number is increased is due to the choice of the dimensionless variables. It should be noticed that the results are satisfactory even for the coarsest mesh (within 5%), showing that stationary flows can be modeled using rather coarse meshes.

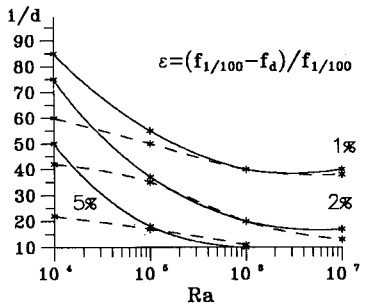


**Fig. 4 Curves of relative iso-error for the cylinder model. $A = 1$, $H_s = 0.75$. Solid lines: stream function maximum, dashed lines: upper heat flux.**

Figure 3 shows some comparisons for temperature and velocity profiles at $Ra = 10^6$ and for two cylinder diameters, 1/20 and 1/70. Results for 1/100 diameter are not given here because no visible difference can be seen between them and the plots for the 1/70 diameter. Also shown are the curves obtained for a heat source term with a 65 × 65 mesh. The temperature profiles on the vertical centerplane (Fig. 3a) show that the temperature tends towards the one for a line heat source when the diameter of the cylinder decreases, though some differences exist below the heat source. The same remark can be made about the vertical component of the velocity profile (Fig. 3b): a nonzero velocity exists at the heat source when it is modeled as a line source. This velocity is close to the velocity maximum for 1/70 diameter in Fig. 3b. Finally, the influence of the cylinder diameter is seen in Fig. 3c, which shows the vertical component of the velocity on the horizontal plane of the wire. While two velocity maxima exist (one on each side of the wire), owing to the no-slip boundary condition on the cylinder and only one for the line heat source, the differences between the models are weak on the major part of the profiles. Obviously, comparisons in the vicinity of the cylinder are better when decreasing the cylinder diameter. It should be noticed that the comparisons with a line source of 1/32 × 1/32 surface are as good as those shown in Fig. 3, except for the source temperature which is lower (see Table 1).

Figures 4 and 5 give more general results for steady flows. Figure 4 shows the relative errors of two variables when the cylinder diameter is increased from $d = 1/100$ to 1/10 for various Rayleigh numbers. Solid lines are for the maximum of the stream function $\psi_{max}$, while dashed lines are for the heat flux through the top wall, $\bar{\phi}$. These are the 1, 2, and 5% iso-error curves, the reference being the cylinder of 1/100 diameter. First, for $Ra \leq 10^5$, the motion is in the so-called conduction and transition regimes for which heat is mainly transferred by conduction. For $Ra = 10^4$, more than 65% of the heat is transferred to the bottom wall (see Table 2). Then the temperature field is not very sensitive to the diameter variation. The relative errors of the upper heat flux for $d = 1/60$ and $d = 1/20$ (compared to the 1/100 diameter) are close

to 1 and 5%, respectively. On the contrary, great discrepancies appear for the stream function owing to the low velocity of the motion. The cylinder is then an obstacle to the fluid motion all the more so as the velocity field weakens, and the flow is greatly affected by the size of the cylinder. The relative error of the stream function for $d = 1/60$ is about 4% and reaches 17% for $d = 1/20$. Second, in the boundary-layer regime for which heat is mainly convected downstream by the plume, discrepancies are smaller. And it seems that an asymptotic value of the diameter is reached for a given error, 1/40 for 1% and 1/20 for 2%. It occurs for a Rayleigh number close to $10^6$, i.e., the beginning of the boundary-layer regime. Table 2 gives further insight into these conclusions. This table shows for the 1/10 and 1/100 diameters the maximum of the stream function and the upper heat flux for various $Ra$ numbers. It appears that the relative errors (given in parentheses) between these two diameters increase as the Rayleigh number becomes smaller. But, it can be noticed that the heat flux errors are always lower than those of the stream function.

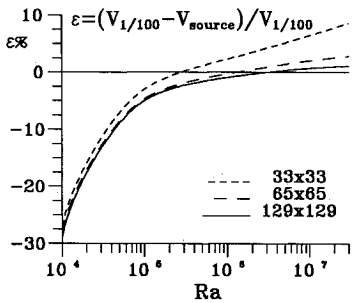


**Fig. 5 Curves of relative error for different mesh sizes of the source term model. The reference is the $d = 1/100$ cylinder. $A = 1$, $H_s = 0.75$.**

**Table 2 Characteristic values of the cylinder model, $A = 1$, $H_s = 0.75$**

| $Ra$ | $d$ | $\psi_{max}$ | | $\bar{\phi}$ | |
|---|---|---|---|---|---|
| $10^4$ | 1/10 | 0.57 | (47%) | 0.302 | (11%) |
| | 1/100 | 0.84 | | 0.334 | |
| $10^5$ | 1/10 | 5.34 | (10.5%) | 0.610 | (10%) |
| | 1/100 | 5.90 | | 0.669 | |
| $10^6$ | 1/10 | 17.52 | (5%) | 0.758 | (4.7%) |
| | 1/100 | 18.40 | | 0.794 | |
| $10^7$ | 1/10 | 45.28 | (3.5%) | 0.812 | (2.2%) |
| | 1/100 | 46.82 | | 0.830 | |

The relative errors are given in parentheses.

The diameter of the line heat source plays a major role in the conduction and in the transition regimes, and has only a minor influence in the boundary-layer regime.

Figure 5 presents the evolution of the relative error with the Rayleigh number for the source term model and for the three mesh grids used, 33 × 33, 65 × 65, and 129 × 129. The comparisons have been done for the maximum of the vertical component of the velocity which is always on the vertical centerplane of the vessel. The reference is the cylinder of diameter $d = 1/100$. The height range is $0.5 \leq y \leq 0.7$ depending on the Rayleigh number. The same conclusions as for Fig. 4 can be drawn. The greatest discrepancies are for $Ra = 10^4$, the relative error being around 30%, whatever mesh size is used. This error decreases when the Rayleigh number increases. For the two finest meshes the relative error remains small even for $Ra = 3 \times 10^7$, while it reaches 10% for the coarsest mesh, 33 × 33. Such a magnitude is not due to a lack of precision of the coarse mesh, the grid of the cylinder model being also built over a 33 × 33 grid (see Fig. 1), but to the difference of the heating surfaces of the two models. Nevertheless, it is worth noticing that the curves for the three meshes show the same trends.

Table 3 gives the maxima of relative errors of the vertical velocity component for various depths of immersion, $H_s = 0.25$, 0.5, and 0.75. To minimize the effects of low velocities on the relative errors, the reference is the maximum of the velocity. Furthermore, these computations have been done only for $Ra = 10^6$. For this value, the plume flow is at the beginning of the boundary-layer regime. For higher Rayleigh numbers the results are of the same order, while they are worse for lower Rayleigh numbers (the motion being weaker, see Fig. 5). The first maximum presented in Table 3 is the one on the horizontal plane of the source cylinder (symbolized by H) while the two others are on the vertical centerplane, the one below the cylinder and the one above (symbolized respectively by VB and VA). The errors on the vertical centerplane are of the same order of magnitude (except for $d = 1/10$), whatever the position of the cylinder. The values are a little bit lower below the source than above. But the size of the cylinders greatly affects the motion, especially for $d \geq 1/30$. On the contrary, the errors on the horizontal plane of the cylinder are not only affected by the size of the cylinder, but also by its location. The errors increase dramatically when the depth of immersion increases. Thus, the errors are below 11 and 6%, respectively, for cylinders of diameters $d \leq 1/50$ and 1/70, whatever the depth of immersion.

The position of the three maxima from the center of the cylinder is also given in Table 3, where $\Delta x$ is on the vertical centerplane and $\Delta y$ on the horizontal plane of the cylinder. At constant depth of immersion, these values show no vari-

**Table 3 Maxima of relative errors (%) of the vertical component of the velocity for various depths of immersion**

| | $H_s = 0.25$ | | | $H_s = 0.5$ | | | $H_s = 0.75$ | | |
|---|---|---|---|---|---|---|---|---|---|
| $d$ | H | VB | VA | H | VB | VA | H | VB | VA |
| 1/10 | 22.9 | 28.6 | 57.4 | 37.9 | 14.2 | 53.8 | 62.3 | 13.5 | 46.4 |
| $\Delta x$ | | 0.064 | 0.090 | | 0.075 | 0.075 | | 0.062 | 0.062 |
| $\Delta y$ | 0.090 | | | 0.103 | | | 0.092 | | |
| 1/20 | 9.4 | 17.6 | 30.5 | 22.2 | 12.9 | 29.9 | 37.8 | 14.5 | 29.1 |
| $\Delta x$ | | 0.041 | 0.064 | | 0.049 | 0.049 | | 0.035 | 0.036 |
| $\Delta y$ | 0.063 | | | 0.075 | | | 0.061 | | |
| 1/30 | 5.4 | 11.7 | 19.1 | 12.6 | 9.3 | 18.6 | 25.6 | 11.8 | 21.4 |
| $\Delta x$ | | 0.041 | 0.064 | | 0.026 | 0.049 | | 0.025 | 0.025 |
| $\Delta y$ | 0.063 | | | 0.075 | | | 0.061 | | |
| 1/50 | 2.2 | 5.7 | 8.8 | 5.2 | 4.8 | 8.4 | 10.6 | 6.8 | 10.5 |
| $\Delta x$ | | 0.041 | 0.064 | | 0.026 | 0.049 | | 0.025 | 0.025 |
| $\Delta y$ | 0.063 | | | 0.075 | | | 0.048 | | |
| 1/70 | 0.9 | 2.6 | 3.9 | 2.2 | 2.3 | 3.7 | 5.6 | 4.0 | 5.7 |
| $\Delta x$ | | 0.041 | 0.064 | | 0.026 | 0.049 | | 0.025 | 0.025 |
| $\Delta y$ | 0.063 | | | 0.075 | | | 0.048 | | |

$Ra = 10^6$, $A = 1$, $\Delta x$, $\Delta y$ positions of the maxima from the center of the cylinder.

ation for $d < 1/20$. For greater diameters, the maxima are slightly shifted away. This demonstrates, rather surprisingly, that the influence area of the diameter on the surrounding fluid motion is rather narrow. But it seems that the depth of immersion of the wire has some influence on the motion. The deeper the heated wire, the smaller is its influence area on the vertical extension (from $\Sigma \Delta x = 0.105$ for $H_s = 0.25$ to 0.05 for $H_s = 0.75$). No general rule seems to be applicable on the horizontal extension.

*Periodic Flows*

The effect of the mesh size on the onset of periodic flows is first examined for the case of a line heat source (Table 4). The flow undergoes a supercritical Hopf bifurcation point to a periodic motion. This kind of bifurcation is characterized by a very slow growth rate of the perturbation amplifications. These perturbations are generated by the round-off errors during the computations. The closer the Rayleigh number is to the critical value, the longer it takes to reach established periodic motion. To insure independence of the periodic motions on the time step, the solutions have been computed for two different time steps ($\Delta t = 10^{-4}$ and $5 \times 10^{-5}$), but only for the two coarsest meshes. Frequencies have been found within 1% for both meshes. Because hundreds of thousands of iterations are needed to reach established periodic motion through supercritical Hopf bifurcations, the 129 × 129 mesh flow has been computed only once. Indeed, computations for such a fine mesh are too CPU-time consuming. Nevertheless, characteristics of the periodic motion are very similar to those found for the 65 × 65 mesh, which gives us confidence in these results.

The flow was found periodic at $Ra = 3.1 \times 10^7$ with a 129 × 129 mesh. But the flow was stationary at this Rayleigh number with a 65 × 65 mesh, in spite of the computations having been performed over more than 280,000 time steps (or a reduced time $t = 11.2$). It became periodic at $Ra = 3.2 \times 10^7$. On a 33 × 33 mesh, the flow was found steady up to $Ra = 6 \times 10^7$. There is nothing surprising in the instabilities setting in at lower $Ra$, because refinements of accuracy only shift bifurcation points without qualitatively affecting the results. This is shown from the values of the frequency which are within 7% (Table 4). All these computations were performed in double precision on IBM 3090 600/VF.

For the cylindrical heat source, calculations have been done only for one cylinder diameter $d = 1/70$; the computations being too time consuming at such a high Rayleigh number on an entry-level workstation. The Rayleigh number at which instabilities occur is $Ra = 7 \times 10^7$, and the system is then attracted to a limit cycle representing a periodic motion of frequency $f = 357 \pm 38$. These values are close to those found for a heat source of 1/32 × 1/32 surface ($f = 336.9 \pm 0.3$ at $Ra = 7 \times 10^7$). The main parameter driving the onset of the perturbations is the mesh size and not the wire size and, as can be seen in Fig. 1, the finite element mesh is built over a 33 × 33 grid.

**Rectangular Vessels of Aspect Ratio 2**

Different kinds of bifurcation were shown by Desrayaud and Lauriat[14] to take place in vessels of aspect ratio greater than 1 according to the depth of immersion. For depths of immersion lower than the width, i.e., $H_s < 1$, the flow undergoes a supercritical Hopf bifurcation. The periodic motion is of low frequency, with the plume setting in motion the fluid

**Table 4 Onset of periodic motion in square vessel for a line heat source $H_s = 0.75$**

| Grid | $Ra$ | Frequency | Computer |
|---|---|---|---|
| 33 × 33 | $6 \times 10^7$ | 319.8 ± 08 | IBM 3090/VF |
| 65 × 65 | $3.2 \times 10^7$ | 299.7 ± 03 | |
| 129 × 129 | $3.1 \times 10^7$ | 307.6 ± 06 | |

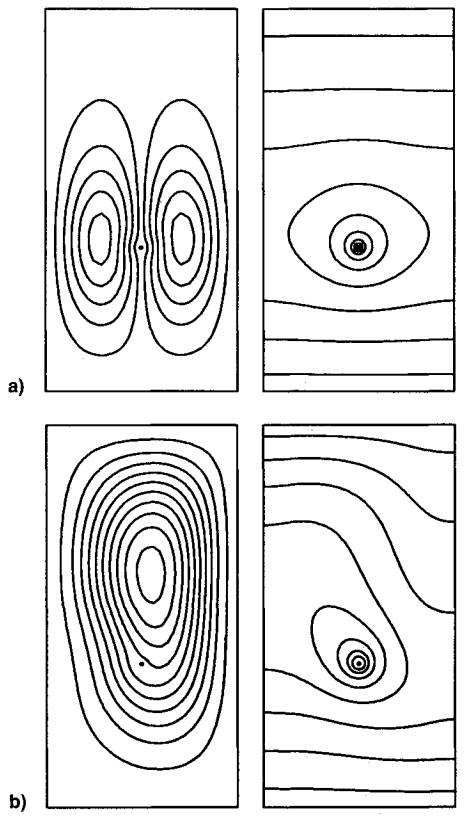


**Fig. 6 Streamlines and isotherms of steady convection driven by a heated wire immersed at $H_s = 1.25$, $d = 1/70$, $A = 2$: a) $Ra = 2 \times 10^3$ and b) $Ra = 6 \times 10^3$.**

below the wire. No comparisons are available for this flow, the bifurcation being a normal Hopf point of the same kind as the one carried out previously for square vessels.

For depths of immersion greater than the width of the vessel, i.e., $H_s > 1$, a pitchfork bifurcation occurs first. The thermal plume does not penetrate into the whole height of the vessel at low Rayleigh numbers, and an unstable linearly stratified layer sets in above the plume (Fig. 6a). Then, two steady solution branches bifurcate from the symmetric solution (Fig. 6b). This corresponds to the deflection of the plume towards one of the vertical surfaces (left or right). These two mirror steady solutions are stable and equally probable. For higher Rayleigh numbers, a subcritical Hopf bifurcation sets in. Perturbations arise with finite amplitude and the motion oscillates between the two asymmetric stationary solutions of the pitchfork branches. Comparisons have been performed for a depth of immersion $H_s = 1.25$, greater than the width.

*Steady Flows*

At low Rayleigh numbers, the heat is transferred mainly by conduction to the horizontal walls, while a very weak motion exists around the plume. Indeed, the isotherms are quasicircular around the heated cylinder (Fig. 6a). Figure 7 presents the vertical component of the velocity (Fig. 7a) and the temperature (Fig. 7b) on the vertical centerplane of the vessel for symmetric steady flows ($Ra = 2 \times 10^3$). Great discrepancies are visible for the velocity owing to the presence of the cylinder. Contrary to what has been found at high Rayleigh numbers and for a wire near the bottom surface (Fig. 3b), there are now two velocity maxima of the same order for the heat flux cylinder (solid lines), indicating that a weak motion sets in below the wire (Fig. 6a). Obviously, there is only one velocity maximum for the line heat source (dashed lines) located close to the source. In addition, the velocities are much lower compared to the ones of Fig. 3b. On the other hand, similar profiles exist for the temperature, owing to the way in which heat is transferred—by conduction. Neverthe-

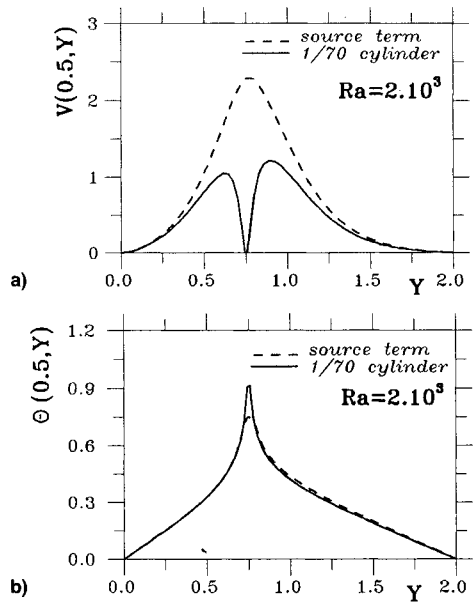


**Fig. 7 Profiles of the a) vertical component of the velocity and b) temperature on the vertical centerplane, $Ra = 2 \times 10^3$, $H_s = 1.25$, $A = 2$, $d = 1/70$.**

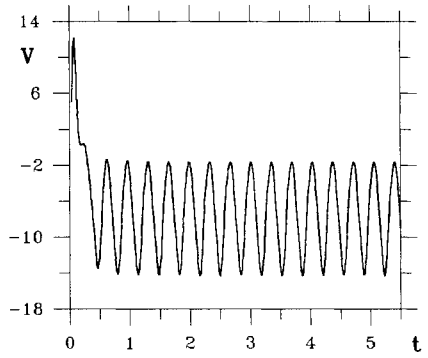


**Fig. 8 Time history of a local variable $V(0.25, 1.5)$ in the case of a heated cylinder of diameter $d = 1/70$, $A = 2$, $H_s = 1.25$, $Ra = 2 \times 10^4$.**

less, some discrepancies can be observed in the vicinity of the heated wire, the heating surface of the source term ($1/32 \times 1/32$) being different from the cylinder's ($d = 1/70$).

At $Ra = 6 \times 10^3$, the unstable linear temperature gradient above the plume produces a deflection of the plume towards one of the vertical walls (Fig. 6b). Despite the poor agreement found for velocity profiles, this deflection occurs for both models at the same Rayleigh number ($Ra = 6 \times 10^3$).

*Unsteady Flows*

Finally, Fig. 8 presents the transient evolution from stationary asymmetric flow at $Ra = 6 \times 10^3$ to $Ra = 2 \times 10^4$ for the case of a 1/70 heated cylinder through a subcritical bifurcation. The transition can be easily detected since the oscillations arise with a finite amplitude. Figure 8 shows the time evolution of the vertical component of the velocity at point $M(0.25, 1.5)$. The motion reaches immediately a limit cycle, representative of a low-frequency periodic flow. The same trend can be seen for both models (the evolution of the source term is not presented here), and the frequencies are in very close agreement. At $Ra = 2 \times 10^4$, the frequency is $f = 3.1 \pm 0.1$ for the case of a local heat source and $f = 3.0 \pm 0.2$ for a 1/70 cylinder.

## Conclusions

We have proposed a concept of modeling a heated wire inside rectangular vessels that is much simpler to construct and is less CPU time consuming. Comparisons with a usual way of modeling heated wire, as a finite diameter cylinder using a finite elements method, have been dealt with.

First, for steady flows at low Rayleigh numbers, in the so-called conduction and transition regimes, a very weak convective flow takes place in the whole vessel. Great discrepancies appear between the two velocity fields. These are mainly due to the weak motion, and the cylinder influence extends far from its location. The temperature field is not affected by the existence of an obstacle, the heat being mainly transferred by pure conduction.

At high Rayleigh numbers, in the boundary-layer regime, strong steady fluid circulation occurs above the line source while a relatively stagnant zone exists below. Velocity fields are close together, except just above the cylinder. The heat is now convected in a well-defined plume, and only weak differences on the isotherms appear in the stagnant zone. Furthermore, it has been shown that there exists only a narrow evolution of the influence of the cylinder size (if $d < 1/20$) on the surrounding fluid motion. But, in the boundary-layer regime, a fundamental parameter is the depth of immersion and the deeper is the heated wire, the smaller is its influence.

Bifurcations in rectangular vessels occur as pitchfork bifurcation, sub- and supercritical Hopf points depending on the depth of immersion, aspect ratio, and Rayleigh number. It has been demonstrated that both models show similar dynamical behavior with very close frequencies—whatever the type of bifurcation points—and rather surprisingly, even for low critical Rayleigh numbers.

In conclusion, these calculations demonstrate that modeling a heated wire as a source term in the energy equation can be a useful tool for investigating complex plume flow situations. Owing to its simplicity, flexibility, and lower computation times, we are now in a position to apply this method to laminar-turbulent transition of plume flows and three-dimensional laminar meandering plume motions.

## Acknowledgments

The authors would like to acknowledge support provided by Numerically Intensive Computing Centre (C3NI), a joint project between Ministère de l'Education Nationale-IBM France, through the use of the IBM 3090-600/VF vector computer at the Centre National Universitaire Sud de Calcul (Montpellier, France). The authors also wish to thank the reviewers for their helpful comments which have definitely improved this manuscript.

## References

[1]Fujii, T., "Theory of the Steady Laminar Natural Convection Above a Horizontal Line Heat Source and a Point Heat Source," *International Journal of Heat and Mass Transfer*, Vol. 6, No. 7, 1963, pp. 597–606.

[2]Gebhart, B., Jaluria, Y., Mahajan, R. L., and Sammakia, B., *Buoyancy-Induced Flows and Transport*, Hemisphere, New York, 1988, Chaps. 3, 11.

[3]Noto, K., Matsui, S., and Matsumoto, R., "Observation on Vortex Pair of Plane Thermal Plume in Thermally Stratified Fluid," *Flow Visualization*, Vol. IV, Springer-Verlag, Berlin, 1982, pp. 697–702.

[4]Urakawa, K., Morioka, I., and Kiyota, M., "Swaying Motion of the Buoyant Plume Above a Horizontal Line Heat Source," *Proceedings of the 1st ASME-JSME Thermal Engineering Conference*, (Honolulu, HI), Vol. 3, 1983, pp. 215–220.

[5]Noto, K., "Swaying Motion in Thermal Plume Above a Horizontal Line Heat Source," *Journal of Thermophysics*, Vol. 3, No. 4, 1989, pp. 428–434.

[6]Eichhorn, R., Lienhart, J. H., and Chen, C. C., "Natural Convection from Iso-Thermal Spheres and Cylinders Immersed in a Stratified Fluid," *Proceedings of the 5th International Heat Transfer Conference* (Tokyo), Vol. 3, 1974, pp. 10–14.

[7]Yaghoubi, M. A., and Incropera, F. P., "Natural Convection from a Heated Horizontal Cylinder Submerged in a Shallow Water Layer," *Proceedings of the 6th International Heat Transfer Conference* (To-

ronto), Hemisphere, Vol. 2, 1978, pp. 269–274.

[8]Eichhorn, R., and Vedhanayagam, M., "The Swaying Frequency of Line Source Plumes," *Proceedings of the 7th International Heat Transfer Conference* (München), Hemisphere, Vol. 2, 1982, pp. 407–412.

[9]Forstrom, R. J., and Sparrow, E. M., "Experiments on the Buoyant Plume Above a Heated Horizontal Wire," *International Journal of Heat and Mass Transfer*, Vol. 10, No. 3, 1967, pp. 321–331.

[10]Shorr, A. W., and Gebhart, B., "An Experimental Investigation of Natural Convection Wakes Above a Line Heat Source," *International Journal of Heat and Mass Transfer*, Vol. 13, No. 3, 1970, pp. 557–571.

[11]Pera, L., and Gebhart, B., "On the Stability of Laminar Plumes: Some Numerical Solutions and Experiments," *International Journal of Heat and Mass Transfer*, Vol. 14, No. 7, 1971, pp. 975–984.

[12]Yosinobu, H., Onishi, Y., Amano, S., Enyo, S., and Wakitani, S., "Experimental Study on Instability of a Natural Convection Flow Above a Horizontal Line Heat Source," *Journal of the Physical Society of Japan*, Vol. 47, No. 1, 1979, pp. 312–319.

[13]Lauriat, G., and Desrayaud, G., "Numerical Study of Oscillatory Buoyant Plumes Above a Horizontal Line Heat Source," *Proceedings of the 9th International Heat Transfer Conference* (Jerusalem), Hemisphere, Vol. 4, 1990, pp. 171–176.

[14]Desrayaud, G., and Lauriat, G., "Unsteady Confined Buoyant Plumes," *Journal of Fluid Mechanics* (to be published).

[15]Himasekhar, K., and Bau, H. H., "Thermal Convection Around a Heat Source Embedded in a Box Containing a Saturated Porous Medium," *Journal of Heat Transfer*, Vol. 110, Aug. 1988, pp. 649–654.

[16]Farouk, B., and Shayer, H., "Natural Convection Around a Heated Cylinder Buried in a Saturated Porous Medium," *Proceedings of the 23rd ASME National Heat Transfer Conference* (Denver, CO), Vol. 46, 1985, pp. 181–189.

[17]Beck, J. V., McLain, H. A., Karnitz, M. A., Shonder, J. A., and Segan, E. G., "Heat Losses from Underground Steam Pipelines," *Journal of Heat Transfer*, Vol. 110, Nov. 1988, pp. 814–820.

[18]Golub, G. H., and Meurant, G. A., *Résolution Numérique des Grands Systèmes Linéaires*, Eyrolles, Paris, 1983, Chap. 3.

[19]Desrayaud, G., Le Peutrec, Y., and Lauriat, G., "Low Prandtl Number Convection in a Shallow Cavity," *Notes on Numerical Fluid Mechanics*, Vieweg, Braunschweig, Vol. 27, 1990, pp. 49–56.

[20]Roux, B. (ed.), "Numerical Simulation of Oscillatory Convection in Low-Prandtl Fluids," *Notes on Numerical Fluid Mechanics*, Vieweg, Braunschweig, Vol. 27, Chap. 5, 1990, pp. 263–303.

[21]FIDAP, *Theoretical Manual*, Vol. 1, Version 6.0, Fluid Dynamics International, Inc., Evanston, IL, 1991.